

High efficient 635 nm resonant-cavity light-emitting diodes with modified electron stopped layers

V. V. LYSAK*, C. Y. PARK^a, K. W. PARK^a, Y. T. LEE^{a,b*}

Semiconductor Physics Department, Chonbuk National University, Chonbuk, Republik of Korea

^a*Gwangju Institute of Science and Technology (GIST), Gwangju, Republik of Korea*

^b*Department of Nanobio Materials and Electronics, GIST, Gwangju, Republik of Korea*

The analysis of electro-optical properties of 635 nm InGaP/InGaAlP resonant-cavity light-emitting diodes with AlGaAs mirrors is presented. We show that including the p-doped electron stop layer in both side of active layer improves the efficiency of such device due to increasing the electron capture efficiency in the quantum wells and decreasing the electrical field across the active layer. Theoretical analysis is proved by experimental work.

(Received February 10, 2010; accepted June 16, 2010)

Keywords: Charge carrier processes, Modeling, Semiconductor materials, Quantum wells, Resonant cavity light emitting diodes

1. Introduction

MICRO-DISPLAY based projectors require projection lamps. Currently high intensity discharge (HID) lamps are used. They have a very high luminance, but limited life, and require a color wheel. Light-emitting diodes (LEDs) have a very long lifetime, and don't require a color wheel, which increases the acceptance and flexibility of a color sequential projection display considerably. With an LED illuminator white points and color gamuts can be changed dynamically, and can be optimized to the source material or viewing conditions. The external quantum efficiency η_{ext} is the key performance figure for high-efficiency LEDs [1] and stands for the number of photons generated per injected electron and depends on the fraction of carriers injected in the useful active region η_{inj} , the fraction of spontaneous recombination that is radiative η_{rad} and the extraction efficiency of the generated photons η_{extr} in the form $\eta_{ext} = \eta_{inj}\eta_{rad}\eta_{extr}$. These three contributions are representative for the more or less successive introductions of optimization.

It is at this stage ($\eta_{inj}\eta_{rad} \approx 1$) that it is appropriate to optimize η_{extr} , which is limited to 2–4% by Snell's law for conventional planar LEDs due to the high refractive index contrast between the source material and the surrounding medium. This optimization happened in the early nineties, when cavity optics entered the world of LEDs with the resonant-cavity LED (RCLED). In these devices, the active layer is embedded in a cavity with at least one dimension of the order of the wavelength of the emitted light. Under those circumstances, the spontaneous emission process itself is modified, such that the internal emission is no longer isotropic.

Schubert *et al.* presented the RCLED as a conceptual novel LED in 1992 [2, 3]. From this time the extraction efficiency was improved up to 50 %.

2. Structure description

Like in standard red LEDs, the GaAsP material system is increasingly substituted by the high-quality AlGaInP for use as active medium. Due to the absorbing substrate (GaAs or Ge), the device is preferably top emitting with a cavity sandwiched in between two DBR mirrors incorporating an appropriate current injection design. Devices in the 600- to 650-nm range are described by several research groups, showing η_{ext} up to 10% [4, 5].

Red RCLED with 635 nm of emission wavelength (Fig. 1) consists of 2 Al_{0.5}Ga_{0.5}As / Al_{0.95}Ga_{0.05}As distributed Bragg reflectors (DBR) with 22.5 pairs for bottom and 5 pairs for top DBR. The cavity consists 815 nm thickness In_{0.498}Ga_{0.08}Al_{0.422}P cladding layers, 0.2 % of compressive-strained InGaP 63 nm quantum wells and 0.1% tensile-strained InGaAlP 150 nm barrier due to the low conduction band offset [6-8]. The conduction band offset of lattice matched InGaP/InGaAlP material system as 165 meV is about a half of the conduction band offset of lattice matched InGaAs/AlGaAs material system 350 meV.

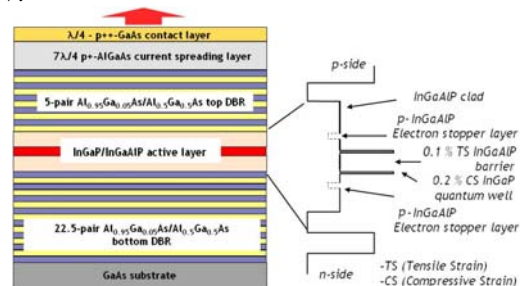


Fig. 1. Red RCLED structure with active layer details.

Due to the low conduction band offset ($\Delta E_c / \Delta E_v \approx 0.4$), electrons in the quantum wells can easily escape from the well reducing internal quantum efficiency in the lattice-matched InGaP/InGaAlP material system. On the top of structure $7\lambda/4n$ $\text{Al}_{0.95}\text{Ga}_{0.05}\text{As}$ current spreading layer with $6 \times 10^{18} \text{ cm}^{-3}$ p-doping is placed to reduce a current uniformity in the active layer and $\lambda/4n$ GaAs contact layer with $1 \times 10^{19} \text{ cm}^{-3}$ p-doping to decrease device resistance and form the ohmic contact. To reduce the electron leakage from active layer the 5 nm p-doped $\text{In}_{0.49}(\text{Ga}_{0.2}\text{Al}_{0.8})_{0.51}$ electron stopped layer (ESL) can be introduced in the cladding layer close to the active layer. Here three structures is compared. First structure does not contain ESL, in second structure ESL is placed on p-cladding and third structure contains ESLs on both p- and n-cladding layers.

3. Numerical simulations models

3.1 Carrier transport and gain calculations

Several software tools were used in the process of designing and optimizing the devices. Besides using the self-consistent model implemented in CrossLight's package APSYS. This software simulates a wide spectrum of electrical, optical and thermal characteristics with the ability to update to new material parameters and calculation algorithms. All important heat sources, i.e. non-radiative recombination, absorption of spontaneous radiation, are taken into account. The main material parameters can be found in the related literature [9].

3.2 Top and bottom mirrors reflectivity

Fast and flexible transfer-matrix-based calculations of the reflection coefficient dependencies (upon wavelength, incidence angle, polarization, layer contrast, layer thickness, number of DBR periods) and of the optical field distributions played an important role in the device development—mostly in the early design stages—and in understanding the angular emission of the RC-LEDs.

We assumed that whole media is homogeneous and plane wave is propagating in the xz plane. With reference to Fig. 2 for the RC-LED model, the top QWS dielectric profile is described by [10]

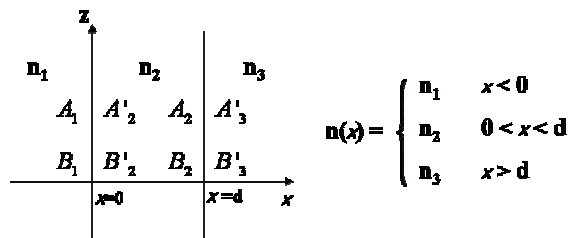


Fig. 2. RC-LED model of top and bottom reflectivity.

Let A_1 and B_1 be the amplitude of the incident and reflected plane wave at $x=0$, and A'_3 and B'_3 be the corresponding amplitudes at $x=d$. These amplitude are related by the 2x2 transfer matrix M_1 . Thus,

$$\begin{bmatrix} A_1 \\ B_1 \end{bmatrix} = M_1 \begin{bmatrix} A'_3 \\ B'_3 \end{bmatrix} \quad (1)$$

For the top QWS reflectivity, matrix M_1 is given by

$$M_1 = \begin{bmatrix} M_{11} & M_{12} \\ M_{21} & M_{22} \end{bmatrix} = D_1^{-1} [D_2 P_2(\lambda) D_2^{-1}]^{N_1} D_3 \quad (2)$$

where N_1 is the number of top pairs of layer and D_i is the dynamical matrix of layer i of refractive index n_i and width d_i . Matrix M_1 accounts for the change in the amplitude of the incident and reflected components of a wave on entry and exit from the medium. D_i is given by

$$D_i = \begin{bmatrix} 1 & 1 \\ n_i \cos \theta_i & -n_i \cos \theta_i \end{bmatrix} \quad (3)$$

$P_i(\lambda)$ is the propagation matrix and it accounts for the phase change experienced by the wave after it has passed through the layer. It is given by:

$$P_i(\lambda) = \begin{bmatrix} e^{j\phi_i(\lambda)} & 0 \\ 0 & e^{j\phi_i(\lambda)} \end{bmatrix} \quad (4)$$

where

$$\Phi_i(\lambda) = n_i d_i \frac{2\pi}{\lambda} \cos \theta_i \quad (5)$$

The reflection coefficient, which is defined as a function of the wavelength λ , can be express in terms of the elements of M_1 by

$$r_1(\lambda) = \frac{M_{21}}{M_{11}} \equiv \sqrt{R_1(\lambda)} e^{j\psi_1(\lambda)} \quad (6)$$

where the reflectivity of the top QWS is given by

$$R_1(\lambda) = |r_1(\lambda)|^2 \quad (7)$$

and

$$\psi_1(\lambda) = \arg[r_1(\lambda)] \quad (8)$$

For the bottom QWS reflectivity, matrix M_2 is given by

$$M_2 = \begin{bmatrix} M'_{11} & M'_{12} \\ M'_{21} & M'_{22} \end{bmatrix} = D_1^{-1} [D_2 P_2(\lambda) D_2^{-1}]^{N_2} D_3 \quad (9)$$

where N_2 is the number of bottom pairs of layer. The reflection coefficient,

$$r_2(\lambda) = \frac{M'_{21}}{M'_{11}} \equiv \sqrt{R_2(\lambda)} e^{j\psi_2(\lambda)} \quad (10)$$

where the reflectivity of the bottom QWS is given by

$$R_2(\lambda) = |r_2(\lambda)|^2 \quad (11)$$

and

$$\psi_2(\lambda) = \arg[r_2(\lambda)] \quad (12)$$

3.3 Calculation of refractive index for $\text{Al}_x\text{Ga}_{1-x}\text{As}$ system

The refractive index of $\text{Al}_x\text{Ga}_{1-x}\text{As}$ system can be given by the Adachi model [11]:

$$n^2 = A(x) \left\{ f(y) + \frac{1}{2} \left[\frac{E_0(x)}{E_0(x) + \Delta_0(x)} \right]^{3/2} f(x_{so}) \right\} + B(x) \quad (13)$$

where

$$f(y) = \frac{1}{y^2} \left[2 - (1+y)^{1/2} - (1-y)^{1/2} \right]$$

$$y = \frac{\hbar\omega}{E_0(x)} \quad y_{so} = \frac{\hbar\omega}{E_0(x) + \Delta_0(x)}$$

$$E_0(x) = \begin{cases} 1.424 + 1.266x + 0.266x^2 & (x < 0.45) \\ 1.656 + 0.215x + 1.147x^2 & (x > 0.45) \end{cases}$$

$$\Delta(x) = 0.34 - 0.131x + 0.071x^2 \quad (eV)$$

$$A(x) = \begin{cases} 6.64 + 16.92x & (x < 0.45) \\ 6.3 + 19.0x & (x > 0.45) \end{cases}$$

$$B(x) = \begin{cases} 9.20 - 9.22x & (x < 0.45) \\ 9.40 - 10.2x & (x > 0.45) \end{cases}$$

Fig. 3 shows dependence of refractive index vs wavelength for two materials $\text{Al}_{0.5}\text{Ga}_{0.5}\text{As}$ and $\text{Al}_{0.95}\text{Ga}_{0.05}\text{As}$. Figure shows that change of refractive index for $\text{Al}_{0.5}\text{Ga}_{0.5}\text{As}$ at operation wavelength is bigger than for $\text{Al}_{0.95}\text{Ga}_{0.05}\text{As}$. Such dispersion will influence on mirrors reflectivity as will be shown in chapter 4.2.

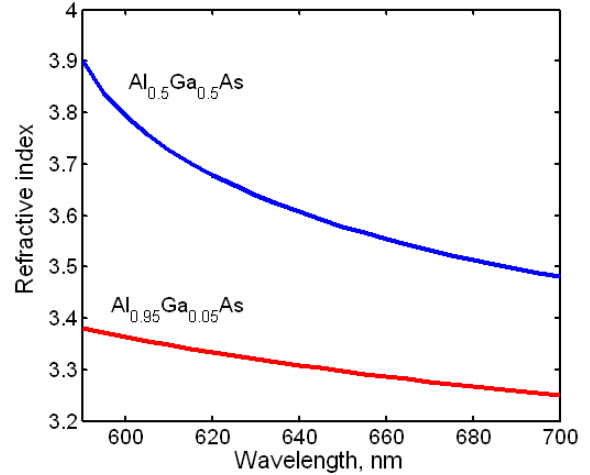


Fig. 3. Wavelength dependence of refractive index for components of RC-LED reflectors.

4. Results and discussion

4.1 Active layer modification

Fig. 4 shows the calculation of conduction band distribution for structures without ESL (green line) compare to device with ESL in p-side (red line) and 2 ESLs in both sides of active layer (blue line). The material and doping concentrations for both layers are depicted on figure. Including the second stop layer to the n-side of structure increase the capture efficiency and makes the energy distribution in the active layer region more uniform.

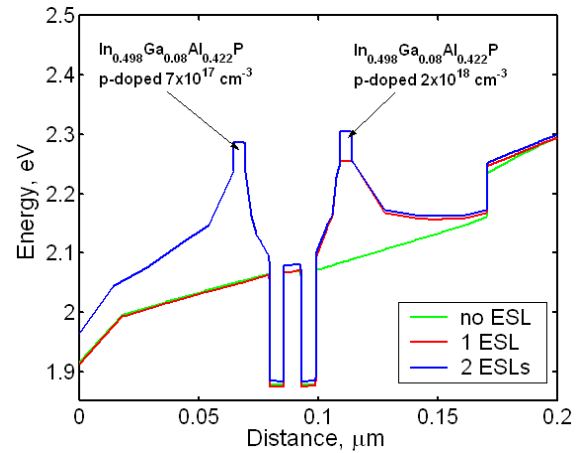


Fig. 4. Conduction band distribution without ESL (green line), with 1 ESL (red line) and with 2 ESLs (blue lines).

The spatial distribution of the electron concentration for different structures is presented in Fig. 5, showing strong inhomogeneous carrier distribution in the SCH layer with including ESL.

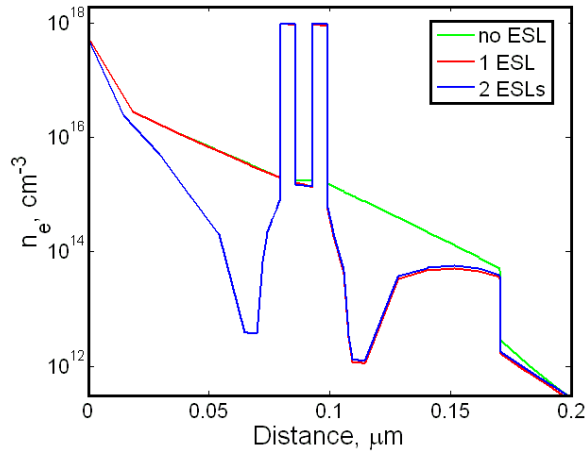


Fig. 5. Electron concentration distribution without ESL (green line), with 1 ESL (red line) and with 2 ESLs (blue lines).

The gain value depends on the population of bound 2D states in each QW which in turn depends on coupling of the 2D states to unbound 3D states. The simple way to consider this fact is to introduce the capture efficiency, as ratio of 2D carrier concentration N_{2D} in a QW to concentration of 3D carriers N_{3D} in a QW, $\eta_{cap} = N_{2D}/N_{3D}$. It will allow in the frame of rate equations to take account of the carrier spatial distribution inhomogeneity and its influence on the LED properties.

Assuming common quasi-Fermi level for 2D and 3D carriers in the well region we can express capture efficiency via (local) capture and escape times as:

$$\eta_{xcap} = \frac{\tau_{xesc}}{\tau_{xcap}} = \frac{\int \rho_{x2D}(E) f_x(E, F_x) dE}{\int \rho_{x3D}(E) f_x(E, F_x) dE}, \quad (14)$$

where $x=e$ (electrons), h (holes); $\rho_{x2D}(E)$ and $\rho_{x3D}(E)$ are the DOS functions of carriers in the well and capture region, respectively; $f_x(E, F_x)$ is the Fermi factor with F_x is the quasi-Fermi level. Using information about energy levels for electrons and holes, quasi-Fermi levels and density-of-states (DOS) we calculate capture efficiency of carriers (electrons(e) or holes(h)) through (13).

Such modification allows increasing the total efficiency of device as shown on Fig. 6. Figure shows slope efficiency (SE) for structure without ESL is equal to 0.452 W/A. If ESL on the p-side cladding layer is introduced SE increased up to 0.483 W/A. When we have a structure with 2 ESLs on both side of active layer SE increased up to 0.598 W/A or 24 % improvement comparing to 1 ESL structure.

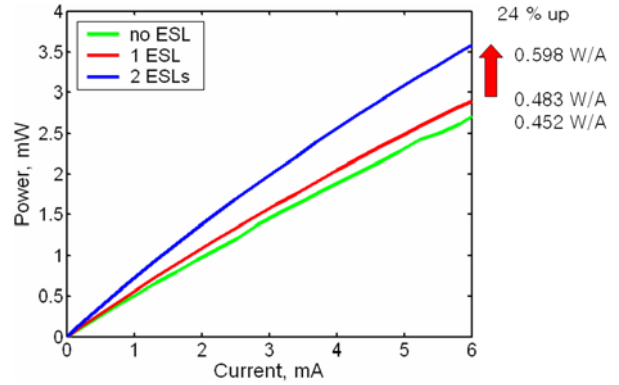


Fig. 6. L-I characteristics for RCLED without ESL (green line), with 1 ESL (red line) and with 2 ESLs (blue lines).

Fig. 7 shows L-I characteristics for 2 ESL structure with different doping values of n-side ESL. If doping concentration is small, we do not see any improvement in SE. In other hand, at large doping concentration QE is saturated. Results show the optimal doping concentration at $7 \times 10^{17} \text{ cm}^{-3}$.

It can be explained by fact that at large doping concentrations the electrons have difficulty to become in the active layer, that increase the resistance of device as shown by I-V characteristics presented in Fig. 8.

4. 2 Mirror reflectivity analysis

Using equations (7) the reflectivity of the bottom Distributed Bragg reflector (DBR) was calculated with and without including wavelength dependency of refractive indices of materials. Results are shown on Fig. 9.

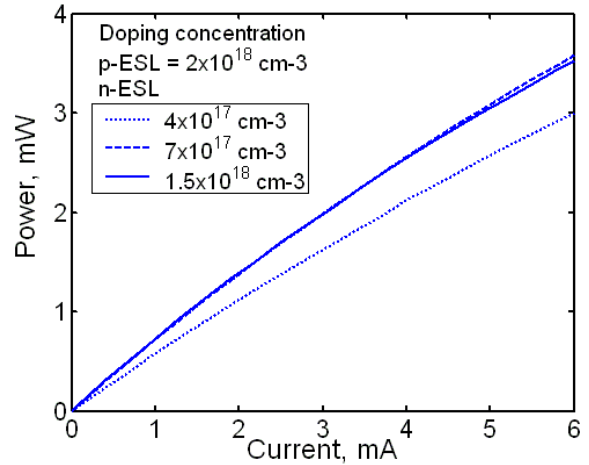


Fig. 7. L-I characteristics for RCLED with 2 ESLs for different doping concentrations of n-ESL.

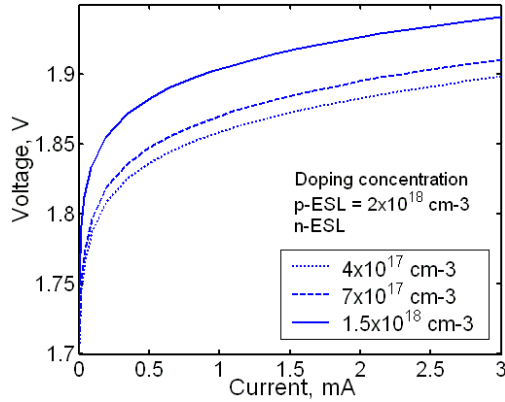


Fig. 8. I-V characteristics for RCLED with 2 ESLs for different doping concentrations of n-ESL.

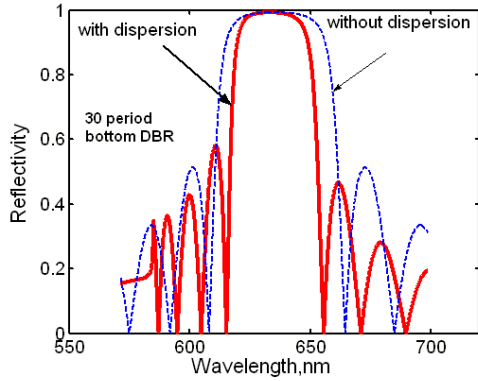


Fig. 9. Reflectivity spectra for 30 period bottom DBR with and without refractive index dispersion.

Results show decreasing the mirror stop-band for model with refractive index dispersion. Using the model with dispersive refractive indices allows finding more suitable values for low and high refractive layer thicknesses, comparable with experimental data as shown on Fig. 10.

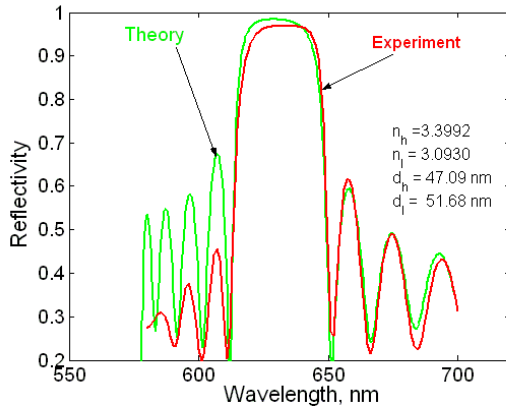


Fig. 10. Reflectivity spectra for bottom DBR at central wavelength of 635 nm and theoretical comparison. Thicknesses of layers are the same for theory and experiment. Also the refractive indices at central wavelength for both layers are presented on figure.

Further analysis also shows a dependence of dispersive refractive indices on central wavelength of mirror with change of layer number as shown on Fig. 11.

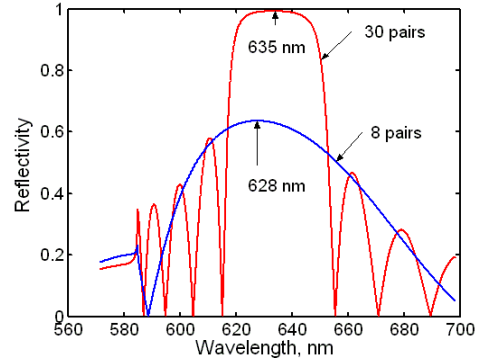


Fig. 11. Reflectivity spectra for top and bottom DBRs.

Results shows decreasing the central wavelength then number of layers is decreased. To solve this problem the layer thicknesses should be slightly modified to get the same central wavelength for both mirrors as shown on Fig. 12.

4.3 Experimental verification

To verify theoretical data, the real device with structure shown on Fig. 1 was grown. Experimental sample of device is presented on Fig. 13.

Results show improvement of SE spectra with introducing the ESL on both sides of active layer that verify our theoretical calculations.

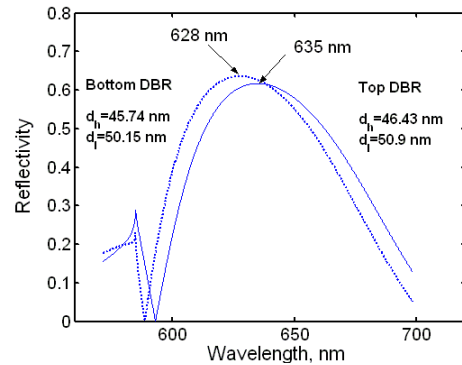


Fig. 12. Reflectivity spectra of top DBR without (central wavelength is 628 nm) and with modified layer thicknesses (central wavelength is 635 nm).

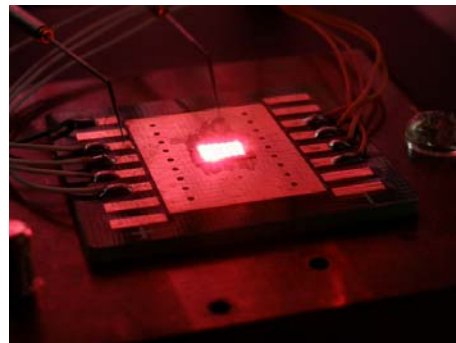


Fig. 13. Experimental sample of red RCLED.

The measured spontaneous emission (SE) spectra are present on Fig. 14. The PL was measured by RPM2000 with using 532nm laser diode which output power is 7 mW at room temperature.

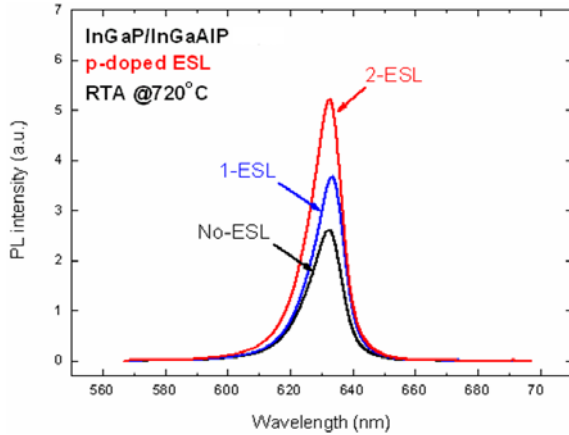


Fig. 14. Spontaneous emission spectra for RCLED without ESL (black line), 1 ESL (blue line) and 2 ESLs (red lines).

5. Conclusions

The electrical and optical properties are analyzed for the 635 nm InGaAlP RCLED with different structures of active layer. Results show, inserting ESL layers in both sides of active layer increases the slope efficiency of L-I characteristic up to 24% due to increasing the electron capture efficiency in the quantum wells.

Reflectivity spectra of both top and bottom DBRs at wavelength 635 nm was theoretically investigated including dispersion relation of refractive index. Results show decreasing the mirror stop-band for model with refractive index dispersion and blue shifting the central wavelength at decreasing the number of layers in the mirror. Comparing with grown mirrors allow receiving the proper thicknesses of layer for bottom mirror ($d_b=457 \text{ \AA}$ and $d_t=502 \text{ \AA}$) and top mirror ($d_b=464 \text{ \AA}$ and $d_t=509 \text{ \AA}$).

The theoretical results were verified experimentally and showed twice increasing the internal quantum efficiency between the structure without ESL and optimized 2 ESL structure.

Acknowledgements

This work was supported by IT RND program of MKE/IITA [2007-F-045-03].

References

- [1] D. Delbeke, R. Bockstaele, P. Bienstman, R. Baets, H. Benisty, *IEEE JSTQE* **8**,189 (2002).
- [2] E. F. Schubert, Y.-H. Wang, A. Y. Cho, L.-W. Tu, G. J. Zyzdik, *Applied Physics Letters* **60**(8), 921 (1992).
- [3] M. R. Krames, M. Ochiai-Holcomb, G. E. Hoefler, C. Carter-Coman, E. I. Chen, I.-H. Tan, P. Grillot, N. F. Gardner, H. C. Chui, J.-W. Huang, S. A. Stockman, F. A. Kish, M. G. Craford, T. S. Tan, C. P. Kocot, M. Hueschen, J. Posselt, B. Loh, G. Sasser, D. Collins, *Applied Physics Letters* **75**(16), 2365 (1999).
- [4] P. Modak, M. D'Hondt, I. Moerman, P. Van Daele, P. Mijlemans, P. Demeester, *Electronics Letters* **37**(6), 377 (2001).
- [5] R. Wirth, C. Karnutsch, S. Kugler, K. Streubel, *IEEE Photonics Technology Letters* **13**, 421 (2001).
- [6] P. Mackowiak, W. Nakwaski, *Journal of Physics D: Appl. Phys.* **34**, 954 (2001).
- [7] M. Dumitrescu, L. Toikkanen, P. Sipilä, V. Vilokkinen, P. Melanen, M. Saarinen, S. Orsila, P. Savolainen, M. Toivonen, M. Pessa, *Microelectronics Engineering* **51–52**, 449 (2000).
- [8] R. P. Schneider Jr., J. A. Lott, M. H. Crawford, K. D. Choquette, *International Journal of High Speed Electronics and Systems Devices* **5**(4), 625 (1994).
- [9] SimuApsys, User's manual and reference manual, version 2008, Crosslight Inc., 2008.
- [10] P. Yen, *Optical waves in Layered Media*, New York, Wiley, 1988.
- [11] S. Adachi, *GaAs and Related Materials*, World Scientific, 1995.

*Corresponding author: Lysak@gist.ac.kr